Internal Waves from Oscillating Objects

B. Voisin

LEGI, CNRS–UJF–INPG,
BP 53, 38041 Grenoble Cedex 9, France
Bruno.Voisin@hmg.inpg.fr

Abstract

An analytical theory is presented for the generation of small-amplitude three-dimensional monochromatic internal waves by an oscillating object. The theory expresses the structure of the waves in terms of the size of the object, the viscosity of the fluid and the time elapsed since the start-up; to this, it adds near-field effect and modification of the added mass of the object by the stratification. Comparison with experiment allows assessment of the relative importance of all five effects.

1. Introduction

Interest in the generation of monochromatic internal waves has recently been revived, owing on one hand to the realization of the importance of internal tides for mixing the ocean (St Laurent and Garrett, 2002), and on the other hand to the advent of digital measurement techniques such as synthetic Schlieren and Particle Image Velocimetry (Dalziel et al., 2000).

Most laboratory experiments so far have dealt with two-dimensional situations, and the agreement with theory has been found satisfactory; see for example Sutherland et al. (1999) for a vertically oscillating cylinder. Lately, tomographic inversion has allowed the generalization of synthetic Schlieren to three-dimensional axisymmetric situations (Onu et al., 2003), a generalization applied by Flynn et al. (2003) to a vertically oscillating sphere. In doing so, a discrepancy has been revealed between experiment and theory.

The present paper proposes amendments to the theory, in order to remove the discrepancy. Three effects are considered: interference with transients produced by the start-up of the motion; near field; modification of the added mass of the oscillating object by the stratification. The exposition is focused on the comparison with Flynn et al. (2003); the details of the theory will be presented elsewhere (Voisin, 2007a, b).

2. The classical theory revisited

In a uniformly stratified fluid of buoyancy frequency N, an object of characteristic radius a generates monochromatic internal waves by oscillating at frequency $\omega < N$ with surface velocity $\mathbf{U}(\mathbf{x})\mathrm{e}^{-\mathrm{i}\omega t}$. The waves vary with time through the factor $\mathrm{e}^{-\mathrm{i}\omega t}$, which is implicit in the following. Wave beams are formed, on a double cone of vertical axis, apex at the object and semi-angle $\theta = \arccos(\omega/N)$. Conical polar coordinates $(x_\pm, \varphi, z_\pm)$ are introduced, with φ the azimuthal angle, $\pm z_\pm$ the direction of energy propagation and $x_\pm$ the direction of phase propagation. In terms of the cylindrical polar coordinates $(r_\mathrm{h}, \varphi, z)$, we have

$$x_\pm = r_\mathrm{h}\cos\theta \mp z\sin\theta, \qquad z_\pm = \pm r_\mathrm{h}\sin\theta + z\cos\theta. \tag{1}$$

The coordinates (x_+, φ, z_+) are used in the upper half-space $z > 0$ and the coordinates (x_-, φ, z_-) in the lower half-space $z < 0$, so that $\pm = \operatorname{sign} z$.

2.1. Calculation of the waves

The classical approach to this problem dates back to Lighthill (1978, §4.10): the oscillating object is represented by a source term in the wave equation, say, a source of mass releasing the volume $q(\mathbf{x})$ of fluid per unit volume per unit time, and the waves are calculated in the far field. An integral over the transverse wavenumber $k_\pm$ is obtained, namely, for the velocity disturbance,

$$\mathbf{u} \sim \pm \frac{\mathbf{e}_{z_\pm}}{2^{5/2}\pi^{3/2}} \left(\frac{\cot\theta}{|z_\pm|} \right)^{1/2} \mathrm{e}^{-\mathrm{i}\pi/4} \int_0^\infty k_\pm^{1/2} q_\pm(k_\pm, \varphi, 0) \mathrm{e}^{\mathrm{i}k_\pm x_\pm} \, \mathrm{d}k_\pm, \tag{2}$$

with $\mathbf{e}_{z_\pm}$ a unit vector along the $z_\pm$-axis and $q_\pm(k_\pm, \varphi_k, m_\pm) = q(\mathbf{k})$. Hereinafter Fourier transforms are defined as $f(\mathbf{k}) = \int f(\mathbf{x}) \exp(-\mathrm{i}\mathbf{k}\cdot\mathbf{x}) \, \mathrm{d}^3k$.

This integral, however, diverges along the wave rays tangent to the surface of the object. Viscosity comes into play (Lighthill, 1978, §4.10), attenuating each Fourier component at the rate $\beta k_\pm^3$ per unit distance along rays, with ν the kinematic viscosity and

$$\beta = \frac{\nu}{2\omega \tan\theta}. \tag{3}$$

Unsteadiness comes into play as well (Voisin, 2003), preventing, at time t after impulsive start-up, each Fourier component to travel further than a distance $1/(\alpha k_\pm)$ along rays, with

$$\alpha = \frac{1}{\omega t \tan\theta}. \tag{4}$$

The velocity disturbance becomes (Voisin, 2007a)

$$\mathbf{u} \sim \pm \frac{\mathbf{e}_{z_\pm}}{2^{5/2}\pi^{3/2}} \left(\frac{\cot\theta}{|z_\pm|} \right)^{1/2} \mathrm{e}^{-\mathrm{i}\pi/4} \int_0^{1/(\alpha|z_\pm|)} \mathrm{e}^{-\beta k_\pm^3 |z_\pm|} k_\pm^{1/2} q_\pm(k_\pm, \varphi, 0) \mathrm{e}^{\mathrm{i}k_\pm x_\pm} \, \mathrm{d}k_\pm. \tag{5}$$

Transitions take place, as the waves propagate away from the source, between a bimodal regime governed by the spectrum of the source and a unimodal regime governed by either viscosity (Ivanov, 1989; Makarov et al., 1990; Chashechkin et al., 2001) or unsteadiness. The names 'bimodal' and 'unimodal' refer to the transverse profile of velocity amplitude: a bimodal profile exhibits two peaks on either side of the axis of the wave beam, and a unimodal profile a single peak at the axis.

The transitions are illustrated in figure 1. They are characterized by two parameters,

$$\sigma_\mathrm{v} = \frac{(\beta|z_\pm|)^{1/3}}{a} = \left(\frac{|z_\pm|/a}{Re \tan\theta} \right)^{1/3}, \qquad \sigma_\mathrm{u} = \frac{\alpha|z_\pm|}{a} = \frac{|z_\pm|/a}{\omega t \tan\theta}, \tag{6}$$

defined as the ratios of the length scales of the problem, with $Re = 2\omega a^2/\nu$ the Reynolds number (see e.g. Batchelor, 1967, §5.13). In the $(\sigma_\mathrm{u}, \sigma_\mathrm{v})$-plane a transition diagram may be drawn (figure 2), in which the boundary between the bimodal and unimodal zones is defined, for the quantity considered, by the largest distance $|z_\pm|$ at which the concavity of the transverse amplitude profile at the axis $x_\pm = 0$ changes sign (Voisin, 2007a).

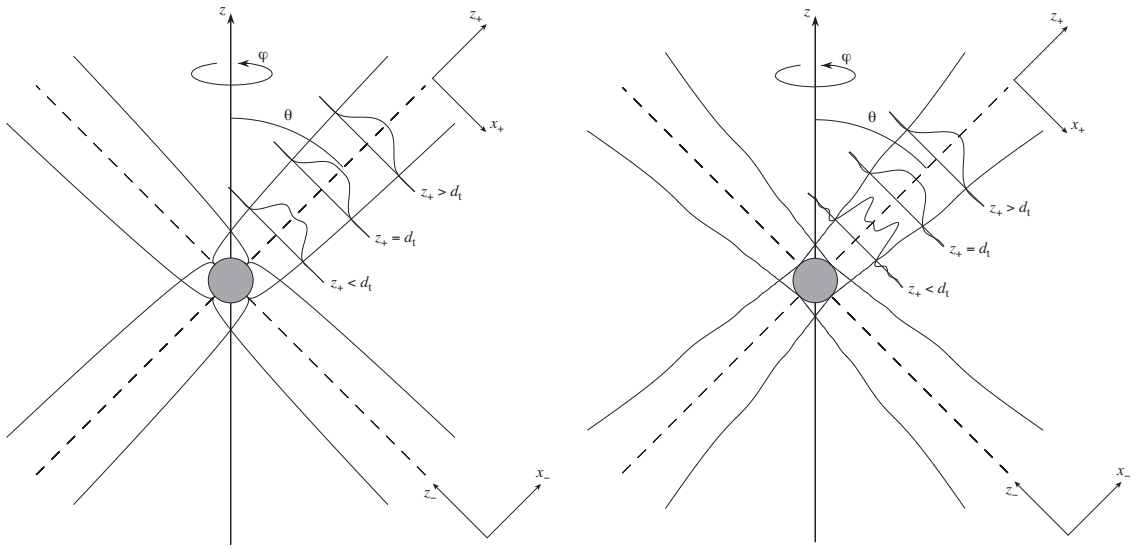

Figure 1. Wave beams from a pulsating sphere, accounting for either viscous effects at $Re = 283$ (left) or unsteady effects at $\omega t = 21$ (right). The wave intensity profile is drawn at three distances z_+ from the sphere, respectively before, at and after the transition from bimodality to unimodality at distance d_t. Distances are drawn to scale with respect to the size of the sphere.

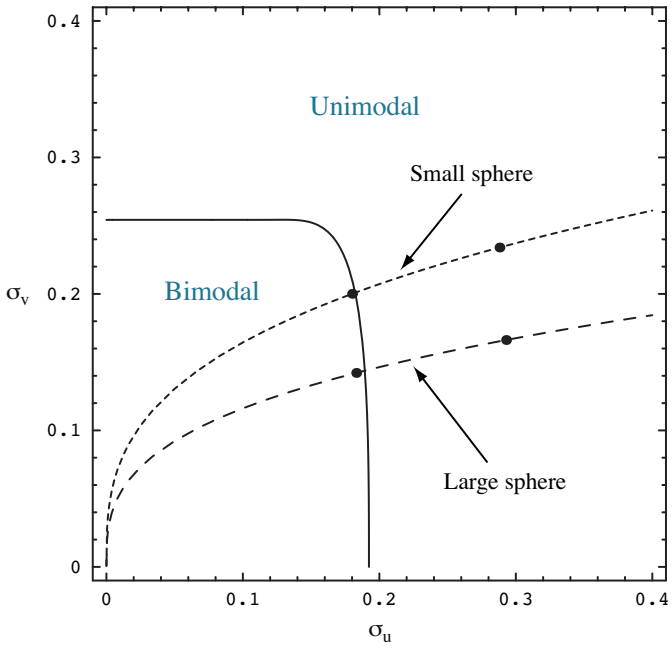

Figure 2. Regimes of internal wave propagation in the experiments of Flynn et al. (2003). The dashed curves represent the trajectories, in the (σ_u, σ_v)-plane, of each experiment as the distance from the oscillating sphere varies, and the points represent the positions of the transverse profiles of figure 3.

2.2. Representation of the oscillating object

Since forcing takes place at the surface S of an oscillating object, the most natural representation of this object is a surface distribution of singularities $q(\mathbf{x}) = \sigma(\mathbf{x})\delta_S(\mathbf{x})$, with δ_S the Dirac delta function of support S. The density $\sigma(\mathbf{x})$ of the distribution satisfies an integral equation, expressing the condition of fixed normal velocity $U_n(\mathbf{x})$ at the surface.

A popular approximation, dating back to Gorodtsov and Teodorovich (1986), Ivanov (1989) and Makarov et al. (1990), consists in borrowing the distribution from the theory of homogeneous fluids, on the assumption that, for small amplitude of oscillation A compared with the radius a of the object, the influence of the stratification is negligible in the vicinity of the object. The integral equation becomes, for $\mathbf{x} \in S$,

$$U_n(\mathbf{x}) = -\frac{1}{4\pi}\frac{\partial}{\partial n}\oint_S \frac{\sigma(\mathbf{x}')}{|\mathbf{x}-\mathbf{x}'|}\,\mathrm{d}^2S', \tag{7}$$

yielding, for a rigid sphere of radius a oscillating at the velocity $\mathbf{U}$,

$$q(\mathbf{x}) = \frac{3}{2}\mathbf{U}\cdot\frac{\mathbf{x}}{r}\delta(r-a), \qquad q(\mathbf{k}) = -6\mathrm{i}\pi a^2\mathbf{U}\cdot\frac{\mathbf{k}}{\kappa}j_1(\kappa a), \tag{8}$$

with $r = |\mathbf{x}|$ and $\kappa = |\mathbf{k}|$. Here $j_1(x) = [\pi/(2x)]^{1/2}J_{3/2}(x) = (\sin x)/x^2 - (\cos x)/x$ and $J_{3/2}(x)$ are spherical and cylindrical Bessel functions, respectively.

3. Beyond the classical theory

3.1. Near-field effects

In the classical approach of §2.1, neither the far-field approximation (2) nor its viscous and unsteady extension (5) have their conditions of validity specified. Going back to the wave equation, and assuming large time $\omega t \gg 1$ and large Reynolds number $Re \gg 1$ but leaving r/a arbitrary, we obtain (Voisin, 2007a)

$$\mathbf{u} \sim \pm\frac{\cos\theta}{8\pi^2}\int_0^{2\pi}\mathrm{d}\varphi_k\,\mathbf{e}_{m_\pm}(\varphi_k)\int_0^{\cos\theta/(\alpha|z|)}\mathrm{d}k_\pm\,\mathrm{e}^{-\beta k_\pm^3|z|/\cos\theta}k_\pm q_\pm(k_\pm,\varphi_k,0)\mathrm{e}^{\mathrm{i}k_\pm\Phi(\varphi_k)}, \tag{9}$$

with

$$\Phi(\varphi_k) = r_\mathrm{h}\cos\theta\cos(\varphi_k-\varphi) \mp z\sin\theta, \tag{10}$$

and

$$\mathbf{e}_{m_\pm}(\varphi_k) = \pm\mathbf{e}_{r_\mathrm{h}}\sin\theta\cos(\varphi_k-\varphi) \pm \mathbf{e}_\varphi\sin\theta\sin(\varphi_k-\varphi) + \mathbf{e}_z\cos\theta. \tag{11}$$

The result (5) is recovered at large distances $|z_\pm|/a \gg 1$. At smaller distances $|z_\pm|/a = O(1)$, two discrepancies arise. First, all the wavenumber vectors satisfying the dispersion relation contribute to the wave field, instead of only those, of azimuthal angle $\varphi_k = \varphi$, associated with group velocity vectors pointing towards the point of observation. Secondly, the viscous and unsteady cutoffs involve the projected vertical distance $|z|/\cos\theta$, instead of the longitudinal distance $|z_\pm|$ along rays. Since $|z|/\cos\theta = |z_\pm \mp x_\pm\tan\theta|$, a transverse asymmetry of the wave beams follows, the waves being more attenuated for $x_\pm < 0$ than for $x_\pm > 0$.

3.2. Added-mass effects

In a stratified fluid, the representation of the oscillating object satisfies, for $\mathbf{x} \in S$,

$$U_n(\mathbf{x}) = -\frac{1}{4\pi(\omega^2 - N^2)^{1/2}} \left(\omega^2 \frac{\partial}{\partial n} - N^2 \frac{\partial}{\partial n_\mathrm{h}} \right) \oint_S \frac{\sigma(\mathbf{x}')}{[\omega^2(\mathbf{x}-\mathbf{x}')^2 - N^2(z-z')^2]^{1/2}} \, \mathrm{d}^2 S'. \quad (12)$$

For a rigid sphere of radius a and velocity $\mathbf{U}$, this integral equation can be solved exactly (Voisin, 2007b). The result is the same (8) as in a homogenous fluid, except for the replacement of the actual velocity $\mathbf{U}$ by the virtual velocity $\mathbf{U}^\star$, of horizontal and vertical components

$$\mathbf{U}_\mathrm{h}^\star = \frac{4/3}{1 + B(\omega/N)} \mathbf{U}_\mathrm{h}, \qquad W^\star = \frac{2/3}{1 - B(\omega/N)} W, \quad (13)$$

varying with frequency according to

$$B\left(\frac{\omega}{N}\right) = \frac{\omega^2}{N^2} \left[1 - \left(1 - \frac{\omega^2}{N^2} \right)^{1/2} \left(\mathrm{i}\frac{\pi}{2} + \operatorname{arccosh} \frac{N}{\omega} \right) \right]. \quad (14)$$

The physical interpretation of this result is a modification of the added mass of the sphere by the stratification, a phenomenon first noticed theoretically by Lai and Lee (1981) and verified experimentally by Ermanyuk (2002) and Ermanyuk and Gavrilov (2003). It is only in the limit $\omega \gg N$ that $B \to 1/3$ and $\mathbf{U}^\star \to \mathbf{U}$, irrespective of the amplitude of oscillation.

4. Comparison with experiment

We apply the above results to the experiments of Flynn et al. (2003), involving two spheres, one small ($a = 1.9$ cm, such that $Re = 350$) and the other large ($a = 3.2$ cm, such that $Re = 1000$). Each sphere starts at time $t = 0$ to oscillate with vertical displacement $-A\sin(\omega t)$, yielding $\mathbf{U} = -\omega A \mathbf{e}_z$. The perturbation ΔN^2 of the squared buoyancy frequency is measured, and its amplitude $|\Delta N^2|$ is obtained by sampling the measurement at sixteen equally spaced times between the start $\omega t = 4\pi$ and the end $\omega t = 6\pi$ of the third period of oscillation, then calculating the root-mean-square average of the samples and multiplying the result by $\sqrt{2}$.

The theoretical perturbation is, for $\omega t \gg 1$ and $Re \gg 1$,

$$\Delta N^2 \sim \pm \mathrm{i} N^2 \frac{A}{a} \frac{(\sin\theta\cos\theta)^2}{1 - B(\cos\theta)} \int_0^{(a\cos\theta)/(\alpha|z|)} \exp\left(-\frac{\beta|z|}{a^3\cos\theta} K^3 \right) \times K^2 j_1(K) J_0\left(K \frac{r_\mathrm{h}}{a} \cos\theta \right) \exp\left(\mp \mathrm{i} K \frac{z}{a} \sin\theta \right) \mathrm{d}K, \quad (15)$$

becoming, in the far field $|z_\pm| \gg a$,

$$\Delta N^2 \sim \pm \frac{\mathrm{e}^{\mathrm{i}\pi/4}}{\sqrt{2\pi}} N^2 \frac{A}{a} \frac{(\sin\theta\cos\theta)^{3/2}}{1 - B(\cos\theta)} \sqrt{\frac{a}{|z_\pm|}} \times \int_0^{a/(\alpha|z_\pm|)} \exp\left(-\frac{\beta|z_\pm|}{a^3} K^3 \right) K^{3/2} j_1(K) \exp\left(\mathrm{i} K \frac{x_\pm}{a} \right) \mathrm{d}K. \quad (16)$$

Based on this far field, the bimodal and unimodal regimes are as represented in figure 2. The boundary between them satisfies $J^2(3, \sigma_\mathrm{u}, \sigma_\mathrm{v}) = J(2, \sigma_\mathrm{u}, \sigma_\mathrm{v}) J(4, \sigma_\mathrm{u}, \sigma_\mathrm{v})$, where

$$J(\mu, \sigma_\mathrm{u}, \sigma_\mathrm{v}) = \int_0^{1/\sigma_\mathrm{u}} \mathrm{e}^{-K^3\sigma_\mathrm{v}^3} K^{\mu-1} J_{3/2}(K) \, \mathrm{d}K. \quad (17)$$

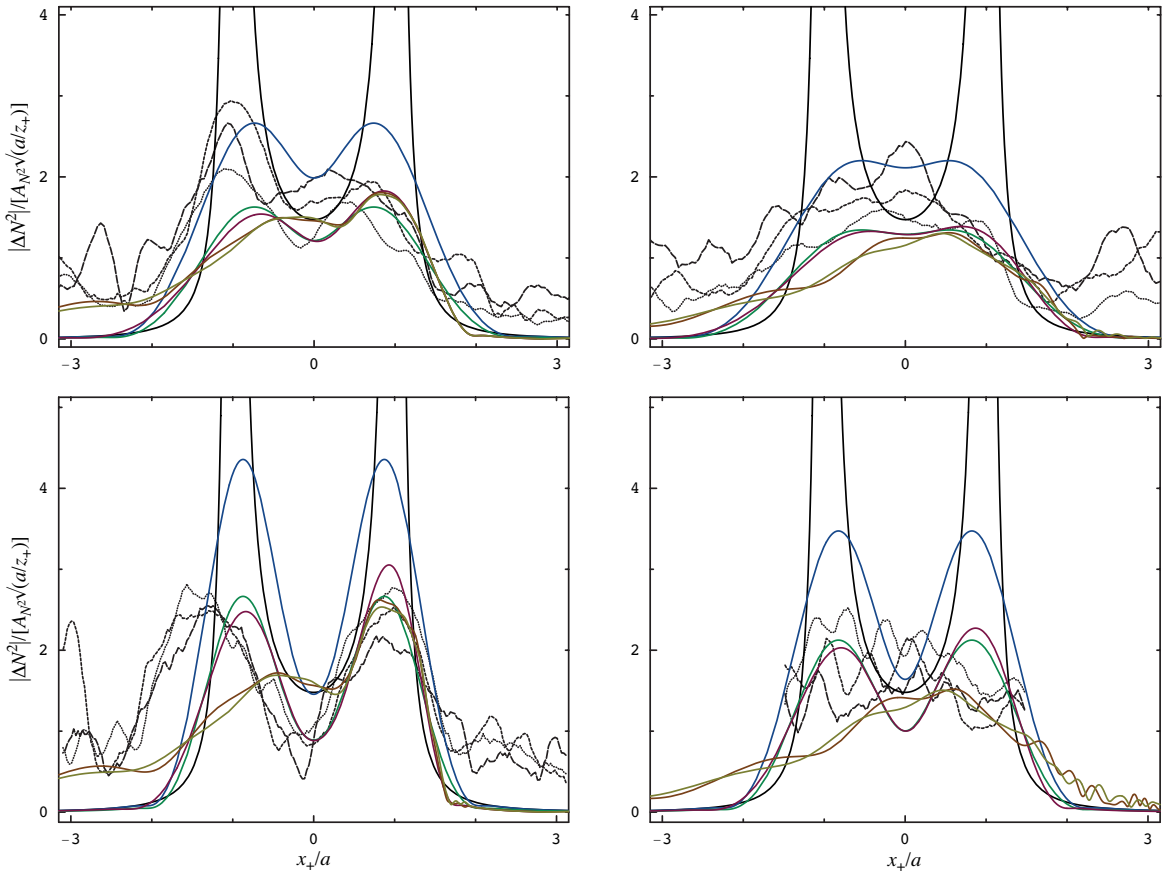

Figure 3. Transverse profiles of $|\Delta N^2|$ at two distances $z_+/a = 5$ (left) and 8 (right) from the small (top) and large (bottom) spheres in the experiments of Flynn et al. (2003). The dashed curves represent the experimental data for three different oscillation amplitudes. The continuous curves represent the theory, starting from the steady inviscid far field (—) and adding cumulatively the effects of viscosity (—), added mass (—), near field (—), unsteadiness (—) and rms (—). The unsteady profiles are calculated at $\omega t = 5\pi$, and the rms profiles are deduced from sixteen samples starting at $\omega t = 4\pi$ and separated by $\pi/8$.

We focus on comparison with figures 8–11 of Flynn et al. (2003), where the amplitude is normalized by $A_{N^2} = (N^2/2)(A/a)\sin\theta\cos\theta$ and where two types of variations are plotted, in the upper beam: transverse profiles at two longitudinal positions $z_+/a = 5$ and 8, and longitudinal variations at two transverse positions $x_+/a = 0$ and -1. The measurements are compared with theory in figures 3 and 4.

Flynn et al. (2003) considered only the size of the sphere and the viscosity of the fluid. Accordingly, with σ_v smaller, at both $z_+/a = 5$ and 8, than its transition value 0.254 for steady waves, the profiles were expected to be bimodal. Inclusion of unsteadiness in figure 2 reveals that the profiles are actually unimodal at $z_+/a = 8$ and just about bimodal at $z_+/a = 5$.

In the theoretical curves, the distinctive influence of each mechanism is visible: inviscid profiles, singular at $x_+ = a$ and $-a$; viscosity, turning the singularities into peaks which broaden as z_+ increases; added mass, diminishing the amplitude by 40 %; near field, breaking the symmetry of the profiles by increasing the peak at positive x_+ and decreasing the peak at negative x_+; unsteadiness, adding oscillations in both the transverse profiles and the longitudinal variations; rms calculation, altering the oscillations all the more as the number of samples is smaller.

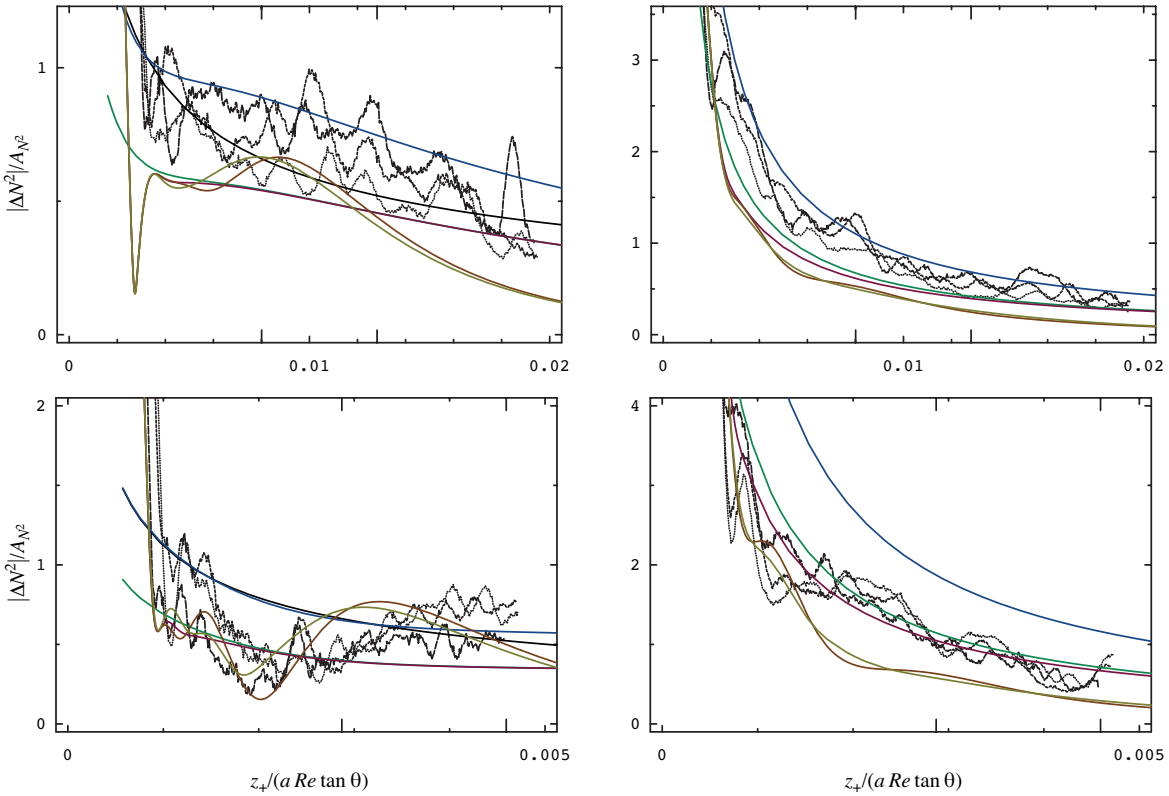

Figure 4. Longitudinal variations of $|\Delta N^2|$ at two positions $x_+/a = 0$ (left) and -1 (right) across the wave beam for the small (top) and large (bottom) spheres in the experiments of Flynn et al. (2003). The mode of representation is the same as in figure 3. The longer tick marks represent the positions $z_+/a = 5$ and 8 of the transverse profiles in figure 3.

In the experimental curves, the dominant effect is the added mass correction, especially for the large sphere. No such correction was required for the two-dimensional experiments of Sutherland et al. (1999) with a vertically oscillating cylinder: the theory was that of Hurley and Keady (1997), taking the inviscid solution of Hurley (1997) obtained by solving exactly the boundary-value problem in a stratified fluid, then rewriting the solution as a wavenumber integral similar to (2) and adding the viscous attenuation factor as in (5); accordingly, the added mass correction was included already. By contrast, for the vertically oscillating sphere, Flynn et al. (2003) started from the solution of Voisin (1991) for a pulsating sphere and differentiated it vertically; in this way, the added mass correction was overlooked.

On top of this, an asymmetry is observed in the transverse profile for the small sphere at $z_+/a = 5$, but this asymmetry goes opposite to that predicted by near-field effects and is absent for the large sphere. The overall noise level of the measurements makes it difficult to assess unsteady effects precisely. These effects, though, seem to provide an explanation for the otherwise unexplained increase of the amplitude at sufficiently large z_+ for the large sphere on the axis $x_+ = 0$.

5. Conclusion

An improved analytical theory of the generation of small-amplitude three-dimensional monochromatic internal waves by oscillating objects has been proposed, built upon the theory of Lighthill (1978, §4.10) and adding three generally overlooked effects: unsteadiness; near field; variation of added mass with frequency. The conditions of validity of Lighthill's theory have been specified:

large distance from the object compared with its size, large time after the start-up compared with the period of oscillation, and large Reynolds number. Comparison with the experiments of Flynn et al. (2003) for a vertically oscillating sphere is encouraging, in that each effect is seen to play a role in certain circumstances, with added mass correction the most significant effect. However, the limitations of the experiments make it impossible, at this stage, to determine precisely which effect is observed in which circumstance, and call for the realization of more detailed experiments.

Acknowledgements

This work has been supported in 2005 by a PATOM grant from the Institut National des Sciences de l'Univers, and in 2006 by a non-thematic grant from the Agence Nationale de la Recherche. The author would like to thank Prof. Bruce Sutherland and Dr Morris Flynn for generously providing their experimental data and helping with their use.

References

Batchelor, G.K. (1967) *An Introduction to Fluid Dynamics*. Cambridge University Press.
Chashechkin, Yu.D., Kistovich, Yu.V. and Smirnov, S.A. (2001) *Environmetrics*, 12:57–80.
Dalziel, S.B., Hughes, G.O. & Sutherland, B.R. (2000) *Exps. Fluids*, 28:322–335.
Ermanyuk, E.V. (2002) *Exps. Fluids*, 32:242–251.
Ermanyuk, E.V. and Gavrilov, N.V. (2003) *J. Fluid Mech.*, 494:33–50.
Flynn, M.R., Onu, K. and Sutherland, B.R. (2003) *J. Fluid Mech.*, 494:65–93.
Gorodtsov, V.A. and Teodorovich, E.V. (1986) *J. Appl. Mech. Tech. Phys.*, 27:523–529.
Hurley, D.G. (1997) *J. Fluid Mech.*, 351:105–118.
Hurley, D.G. and Keady, G. (1997) *J. Fluid Mech.*, 351:119–138.
Ivanov, A.V. (1989) *Izv. Atmos. Ocean. Phys.*, 25:61–64.
Lai, R.Y.S. and Lee, C.-M. (1981) *Int. J. Engng Sci.*, 19:1411–1420.
Lighthill, J. (1978) *Waves in Fluids*. Cambridge University Press.
Makarov, S.A., Neklyudov, V.I. and Chashechkin, Yu.D. (1990) *Izv. Atmos. Ocean. Phys.*, 26:548–554.
Onu, K., Flynn, M.R. and Sutherland, B.R. (2003) *Exps. Fluids*, 35:24–31.
St Laurent, L. & Garrett, C. (2002) *J. Phys. Oceanogr.*, 32:2882–2899.
Sutherland, B.R., Dalziel, S.B., Hughes, G.O. and Linden, P.F. (1999) *J. Fluid Mech.*, 390:93–126.
Voisin, B. (1991) *J. Fluid Mech.*, 231:439–480.
Voisin, B. (2003) *J. Fluid Mech.*, 496:243–293.
Voisin, B. (2007a) Transition regimes of internal wave beams. (In preparation).
Voisin, B. (2007b) Oscillating bodies and added mass for motion in density-stratified fluids. (In preparation).